Materials Horizons

ROYAL SOCIETY OF CHEMISTRY

COMMUNICATION

View Article Online
View Journal | View Issue

Check for updates

Cite this: *Mater. Horiz.*, 2025, **12**, 7033

Received 27th March 2025,
Accepted 9th June 2025

DOI: 10.1039/d5mh00555h

rsc.li/materials-horizons

Designing pores to suppress crack generation at the interface between serpentine interconnects and elastomers for highly durable stretchable electronics†

Seungkyu Lee, [a] Jun Chang Yang *[b] and Steve Park *[a]

Serpentine interconnects enable rigid materials to have high stretchability. They are considered to be very effective architectures to enable stretchable electronics. Therefore, research has primarily focused on exploring serpentine-based designs to enhance the stretchability of the interconnect itself. However, in practical applications, the interfacial cracks caused by repetitive stretching becomes a critical issue if serpentine interconnects are encapsulated within a polymer matrix. Here, we introduce geometrically engineered pores in a polymer matrix to suppress interfacial cracks under stretching. The serpentine interconnects with optimized pores in a polymer matrix improved mechanical stability (strain at failure, fatigue life) and electrical stability compared with those without pores. Furthermore, these strategies enabled the demonstration of a stretchable light-emitting diodes (LED) array and an electrical heater.

New concepts

This work introduces a geometrically guided approach to enhance interfacial mechanical stability in stretchable electronics by embedding engineered pores around serpentine interconnects. Unlike previous efforts that focused primarily on improving the stretchability of the interconnects themselves, our concept addresses the critical (but often overlooked) challenge of interfacial failure between rigid serpentine structures and soft polymer matrices. Strategically placed T-shaped pores in the encapsulating polymer promoted out-of-plane deformation and reduced localized strain, effectively suppressing crack initiation and propagation at the interface. This purely structural design, free of chemical modification or complex fabrication, significantly improved mechanical and electrical durability, achieving stable operation over 15 000 cycles of stretching and 1000 cycles of twisting. Furthermore, the pore architecture was highly versatile, applicable across various serpentine geometries and materials. This concept not only extends the fatigue life of stretchable devices but also enables practical demonstrations such as conformal LED arrays and skin-attachable heaters. The underlying insight lies in transforming the traditionally passive polymer–serpentine interface into an active mechanical element for durability, offering a fundamentally new strategy for engineering long-term, reliable, and stretchable electronics.

Introduction

Stretchable electronics have received huge attention due to their high mechanical compliance and the ability to maintain various functions regardless of the curvature of the attached surface or mechanical deformation.[1,2] Recently, stretchable displays,[3] "electronic skin" with tactile sensing,[4] and medical devices[5] have been demonstrated by introducing geometry designs to inorganic electronics. Various designs, such as serpentine,[6] kirigami,[7] and wrinkling,[8] allow rigid materials-based component (stretchability $<5\%$) to have high stretchability. Among them, the serpentine structure has high stretchability due to its repeated curved shaped, similar to a spring.[9]

To date, various designs to enhance the mechanical properties of serpentine interconnects have been presented. For example, Pang *et al.* designed a fractal-shaped serpentine structure to enhance mechanical flexibility, demonstrating up to 90% stretchability and applying it to electronic skin.[10] Liu *et al.* showed that serpentine interconnects patterned on biocompatible parylene-C films maintained stable impedance even after 5000 repetitive stretching cycles.[11] However, such studies on serpentine structures have consistently focused on improving stretchability without considering the integration with other components (*i.e.*, encapsulation with the polymer matrix).

Despite embedding the serpentine structure in low-modulus materials to avoid mechanical damages (*e.g.*, crack, delamination), repetitive stretching can ultimately lead to crack propagation and device destruction due to the mechanical mismatch of the Young's modulus of the material at the interface between

[a] *Department of Materials Science and Engineering, Korea Advanced Institute of Science and Technology (KAIST), 34141, Republic of Korea. E-mail: stevepark@kaist.ac.kr*

[b] *Smart 3D Printing Research Team, Korea Electrotechnology Research Institute (KERI), Changwon, 51543, Republic of Korea. E-mail: kentya@keri.re.kr*

† Electronic supplementary information (ESI) available: FEM simulation, tensile testing, fatigue testing, strain-at-failure measurement, out-of-plane displacement analysis (Fig. S1–S11 and Table S1). See DOI: https://doi.org/10.1039/d5mh00555h

the polymer matrix and serpentine interconnect. Therefore, it is necessary to design devices that maintain interfacial mechanical stability to achieve high mechanical stability and electrical durability. To address this problem, Uemura *et al.* investigated the dependency of stretchability on encapsulation stiffness by considering the modulus and thickness of an elastomer encapsulating serpentine interconnects.[12] Integrating a low-modulus elastomer layer within the encapsulation can enhance the overall stretchability of the device because this layer can be stretched more extensively. However, using excessively low-modulus elastomers can result in a significant modulus mismatch at the interface with serpentine interconnects, which can negatively affect fatigue life and mechanical stability. Liu *et al.* showed serpentine-shaped electrodes incorporating a sulfhydryl-anchored interface with disordered cones could enhance chemical adhesion between the electrodes and a polydimethylsiloxane (PDMS) film.[13] The electrode exhibited 50% stretchability and a 1.8-fold change in resistance over 200 cycles. However, it had the drawback of being applicable only to specific substrate materials and requiring additional chemical coating treatments. Su *et al.* proposed an overstretch strategy that extended beyond the elastic range of stretchable substrates after bonding to a soft substrate, aiming to double the designed elastic stretchability.[14] However, this strategy can reduce stretchability and induce plastic deformation, making it difficult to return to their initial state after an excessive pre-strain process. Comprehensively, it is required to enhance interface stability without chemical treatments or complex processes. In the present study, we found that pores around serpentine interconnects improved the stretchability and mechanical stability of the stretchable electronic devices. These T-shaped pores were designed to fit into the concave parts of the serpentine interconnect. When the device was stretched or twisted, the T-shaped pores simultaneously expanded (Fig. 1A). Geometrically designed pores dispersed strain-concentrated areas at the interface between the serpentine and elastomer, suppressing crack propagation at the interface.

The serpentine interconnect with pores showed stable mechanical and electrical durability under stretching (30% strain) and twisting (90°). Between the interconnected serpentine structures, there were islands where functional chips could be integrated to enable a variety of applications (Fig. 1B). Stretchable devices remained stable even under stretching and twisting. Because of its stretchable characteristics, it could also be applied to e-skin, conforming seamlessly to the skin. Consequently, we demonstrated a stretchable heater array for human healthcare devices (Fig. 1C).

Results

To make stretchable interconnects, various shapes of interconnects, such as zigzag, horseshoe, serpentine, and hierarchical 3D serpentine-helix, have been investigated.[9,14] These interconnects show high stretchability if used alone. However, if these interconnects are embedded in a polymer, interfacial delamination is likely to occur by excessive or repetitive stretching. Therefore, we placed geometrically designed pores near a serpentine interconnect to suppress interfacial cracks. To prepare a sample, a polyimide (PI) film (thickness: 125 μm) was laser-cut to a serpentine structure (Fig. 2A and Fig. S1, ESI†). Teflon™ was laser-cut to fabricate a mold with a pore design. We aligned the serpentine with the Teflon mold and spin-coated with PDMS as an encapsulation layer. After curing the PDMS, it was removed from the Teflon mold. Tensile tests were conducted on serpentine interconnects without pores (SIOP) and those with O-shaped pores (SIWP1) and T-shaped pores (SIWP2) (Fig. 2B and Fig. S2, ESI†). In the case of the SIOP, an

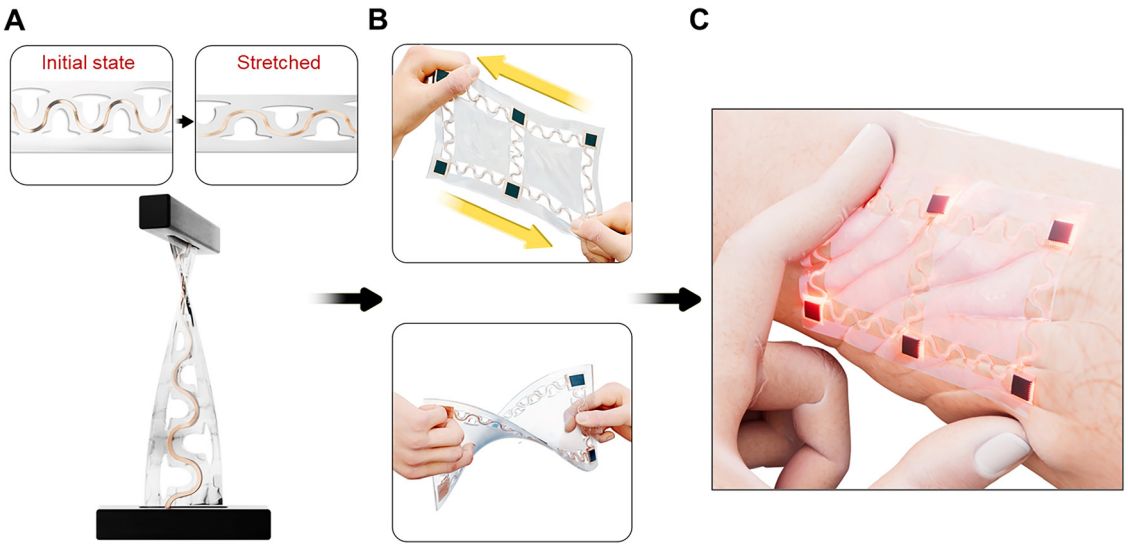

Fig. 1 Stretchable electronics with serpentine interconnects with pores (SIWP) in a polymer matrix (schematic). (A) T-shaped pores reduced lateral strain applied to the serpentine interconnects during stretching and twisting. (B) Stretchable electronics with SIWP operating under stretching (top) and twisting (bottom). (C) A stretchable heater attached to the wrist for electronic-skin (e-skin).

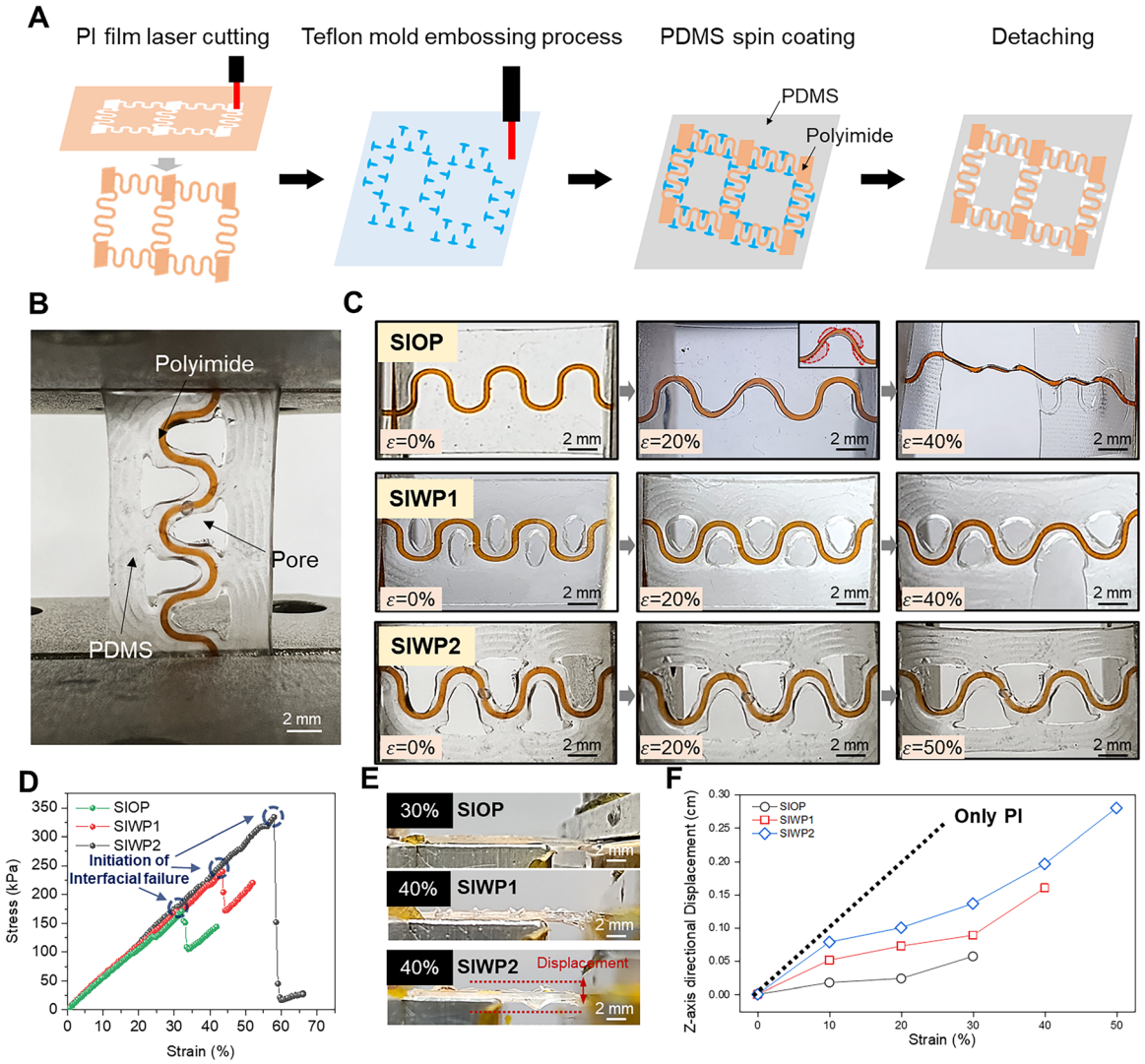

Fig. 2 Fabrication and characterization of the stretchability of serpentine interconnects with pores (SIWP) and without pores (SIOP) in PDMS. (A) Fabrication process for SIWP. (B) Photograph of SIWP in PDMS during tensile testing. (C) Photographs of the tensile tests for SIOP, SIWP with the first pore design (SIWP1), and SIWP with the second pore design (SIWP2) in PDMS. At 20% strain for SIOP, the red dotted area within the inset black dotted box highlights delamination between the serpentine and PDMS. (D) Strain–stress curve for SIOP, SIWP1, and SIWP2. (E) Photographs of the side view of stretched SIOP, SIWP1, and SIWP2. The *z*-axis displacement is defined as the difference between the maximum and minimum values at positions perpendicular to the stretching plane of the serpentine, which is the distance between the two red dotted lines. (F) *Z*-axis directional displacement of polyimide (PI) without PDMS, SIOP, SIWP1, and SIWP2.

interfacial crack (red dotted line) between the serpentine interconnect and the PDMS was observed at 20% strain, leading to interfacial failure before reaching 40% strain (Fig. 2C top). Conversely, in the case of SIWP1, interfacial delamination was not observed up to 40% strain. However, another type of failure was generated from the pore at 43% strain. SIWP2 showed the highest stability up to 58% strain without any other failure. This indicated that T-shaped pores suppressed cracking of the PI/PDMS interface and were stable in themselves, thus increasing stretchability. As shown in Fig. 2D, the strain at failure of SIOP, SIWP1, and SIWP2 was 32%, 43%, and 58%, respectively Here, the inflection points (*i.e.*, sharp drop in stress) in the stress–strain curve indicated strain at failure.[15] In particular, the SIWP2 had high stretchability compared with other forms of SIWP (Fig. S3, ESI†). To observe the deformation process of the serpentine interconnect under stretching, we measured the out-of-plane displacement at 40% strain (Fig. 2E).[11,16] Out-of-plane displacement is an important factor influenced by the stretchability because vertical directional deformation is crucial for structurally stretching rigid materials (*e.g.*, polyimide, polycarbonate).[17,18] Thus, if a serpentine structure is stretched, significant deformation occurs perpendicular to the stretching plane. However, embedding the serpentine interconnect in an elastomer for encapsulation results in the polymer suppressing this perpendicular deformation. This primarily reduces the stretchability and can lead to device failure or a shortened operational lifetime. To address this problem, we positioned geometrically designed pores around the serpentine to promote

free vertical directional deformation. The difference between the lowest and highest *z*-axis position in the side-view is defined as the out-of-plane displacement. As shown in Fig. 2F, the out-of-plane displacement of serpentine interconnects without PDMS (black dotted line) continuously increased with tensile strain. SIWP1 and SIWP2 exhibited relatively high out-of-plane displacements (indicating increased freedom in the *z*-axis direction), with SIWP2 showing higher deformations than SIWP1. In contrast, for SIOP, the out-of-plane displacement was relatively low. As strain increases, the twisting serpentine tears through the elastomer, leading to device failure. This occurs because the PDMS surrounding the serpentine restricts the out-of-plane deformation, inducing cracks at the interface and consequently reducing stretchability. Positioning pores into PDMS facilitates out-of-plane deformation of the serpentine interconnect, which can prevent device failure and improve the overall stretchability of the device.

To date, various serpentine interconnects[10,19,20] have been introduced based on the finite element (FE) simulation to achieve high stretchability, but the understanding of the behaviour of the interconnect embedded in the polymer matrix remains insufficient. The polymer matrix surrounding the interconnect interferes with the movement of the interconnect and causes interfacial cracks. By introducing pores near the serpentine interconnect, the latter was allowed to deform freely regardless of the presence of a polymer. To investigate the process of interfacial failure, we conducted the FE simulation on the PI serpentine interconnect/PDMS matrix (detailed information is described in the Methods section). Fig. 3A–C show FE-simulation images of local strain of the SIOP, SIWP1, and SIWP2 being stretched (lateral strain: 5, 20, 40%). Strain-concentrated areas were generated near the PI/PDMS interface for SIOP due to modulus difference, so interfacial delamination

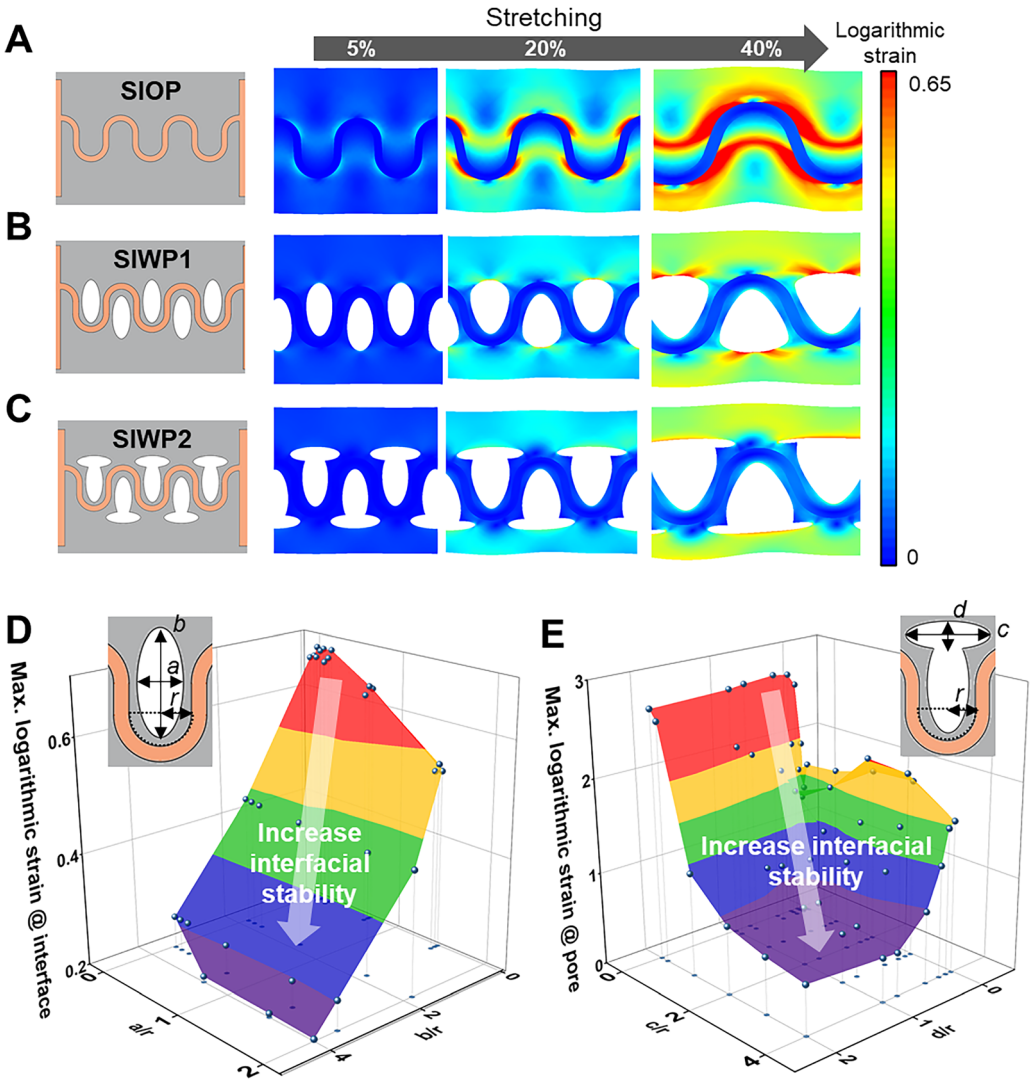

Fig. 3 Interfacial stability at the interface between a serpentine interconnect and polymer matrix. (A–C) Schematic illustration and finite element (FE) simulation image of serpentine interconnects without pores (SIOP) (A), and with pores (O-shape: SIWP1; T-shape: SIWP2) (B and C) in PDMS. (D) Maximum logarithmic strain at the PI/PDMS interface of SIWP1 with differently designed pores. (E) Maximum logarithmic strain at the pores/PDMS interface of SIWP2 with different designed pores.

was likely to occur (Fig. 3A). Conversely, the O-shaped pores minimized the strain on the PI/PDMS interface for SIWP1, effectively preventing interfacial delamination (Fig. 3B). SIWP1 showed the lowest interfacial strain at the PI/PDMS interface when the O-shaped pores were packed into the serpentine interconnects (Fig. 3D). Nevertheless, the interface between pores and PDMS was weak, resulting in a fracture of the PDMS matrix. The strain concentration remained at specific points of the O-shaped pores, which resulted in crack initiation from those points. Therefore, the T-shaped pores not only alleviated strain concentration at the interface but also addressed the drawbacks associated with O-shaped pores (Fig. 3C). This strain-dispersion effect was maximized as the pore size increased, enabling the strain at the pore edge to be minimized to 19% (Fig. 3E). In other words, reducing the maximum logarithmic strain at the pore surface could prevent failure of the pores. We confirmed that the effect was maximized if the pores were fully perforated (Fig. S4, ESI†). Furthermore, geometrically designed pores could be applied to different types of serpentine interconnect (Fig. S5, ESI†).

In addition, it contributed to the fatigue life of the material under stretching. In the fatigue test, a cyclic tensile strain of 30% was applied to SIOP and SIWP2 (Fig. 4A). To measure the number of cycles at which delamination occurred, the relative change in stress was monitored. Due to the viscoelastic properties of the polymer, the stress applied to the device gradually decreased over time in both SIWP2 and SIOP. However, in the case of SIOP in PDMS, delamination was observed at the interface between the serpentine and PDMS during the fourth cycle, as evidenced by a sharp change in the slope of the stress–strain curve (Fig. 4B). For SIWP2, the relative change in modulus remained constant over 15 000 cycles, indicating a stable structure without interfacial cracks and enhanced fatigue resistance (Fig. 4C and Fig. S6, ESI†). Furthermore, SIWP with excellent mechanical interfacial stability contributed to cyclic twisting. To conduct the fatigue test under twisting, a cyclic tensile strain of 30% was applied to SIOP and SIWP2 in PDMS twisted at 45° and 90°, respectively (Fig. 4D). In SIOP in PDMS twisted at 45°, interface fracture occurred at the 124th cycle, while the SIWP2 in PDMS exhibited excellent mechanical stability in both 45° and 90° twisting modes for 1000 cycles without failure (Fig. 4E and F). When twisted at 90° (which involved a greater angle than 45°), the elastomeric viscoelastic properties became more significant, resulting in slightly lower σ/σ_0 values compared to those observed at 45° (Fig. 4F and Fig. S7, ESI†). SIWP2 in PDMS exhibited strong resistance to horizontal and vertical crack propagation, effectively reducing stress concentration at the interface. This resulted in improved elasticity and extended fatigue durability compared to those for SIOP in PDMS.

To operate stretchable electronics, various metals, such as copper (Cu),[21] gold,[22] silver[23] should be deposited on a serpentine interconnect. To ensure stable operation under various repetitive deformations, we used Cu due to its high electrical conductivity (5.96×10^7 S m^{-1}). Here, a 200 nm-thick Cu film (1.394×10^7 S m^{-1}) was deposited on serpentine PI to evaluate electrical stability under unidirectional cyclic tensile test (Fig. 4G). Repeated stretching of the SIOP resulted in cracks

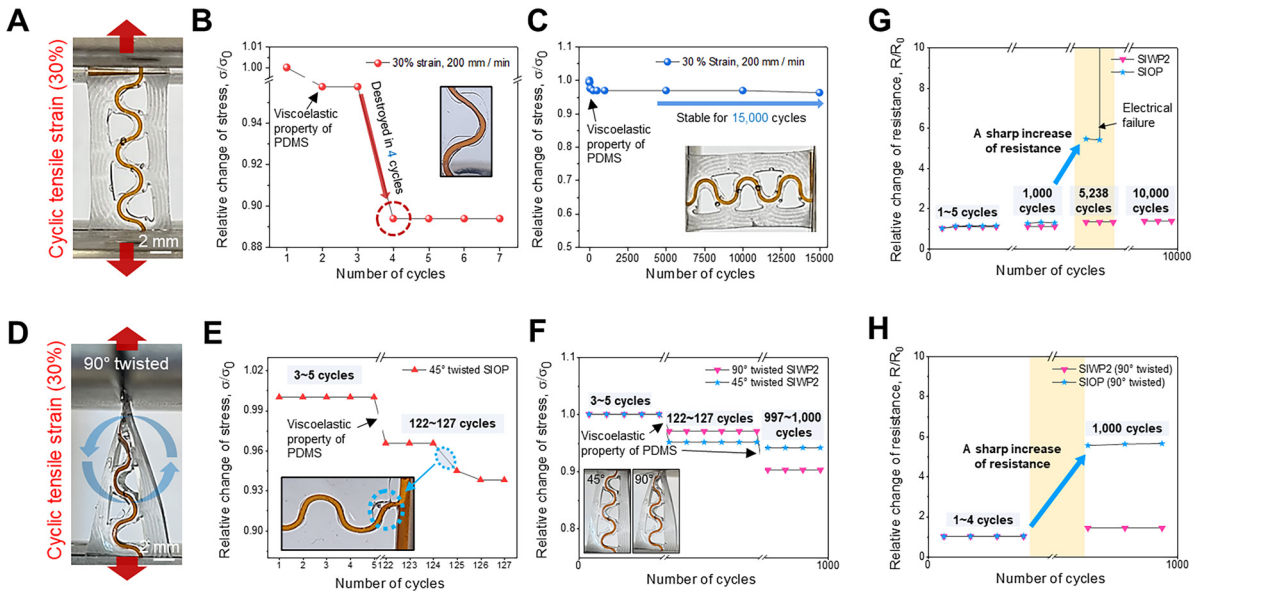

Fig. 4 Mechanical and electrical stability of SIWP2 in PDMS under stretching and twisting compared with SIOP in PDMS. (A) Photograph of SIWP2 in PDMS under 30% cyclic tensile strain. (B and C) Relative change of stress (σ/σ_0) *versus* cycles for both SIOP (B) and SIWP2 (C) in PDMS. The inset image in (B) for SIOP shows a zoomed-in view of the photograph at the fourth cycle, where the device has failed. The inset image in (C) shows no visible crack propagation occurs in SIWP2 in PDMS after 15 000 cycles. (D) Photograph of twisted SIWP2 in PDMS under 30% cyclic tensile strain. (E and F) Relative change in stress (σ/σ_0) *versus* cycles for both SIOP (E) and SIWP2 (F) in PDMS under twisting deformation. The inset image of (E) shows the 45° twisted SIOP at the 125th cycle, where the device has failed. The inset images of (F) show the 45° (left) and 90° (right) twisted SIWP2, both demonstrating its stability (F). (G and H) Relative resistance change (R/R_0) *versus* cycles for SIOP and SIWP2 under stretching (G) and 90° twisting (H).

on the surface of the deposited Cu layer. These cracks were observed using optical microscopy (OM) and scanning electron microscopy (SEM) (Fig. S8, ESI†). SIWP2 deposited with Cu showed minimal resistance changes over 10 000 cycles, ($R/R_0 \approx 1.35$), maintaining values close to the initial cycle. In contrast, SIOP deposited with Cu exhibited a significant increase in resistance, indicating electrical failure of the interconnect. This could be attributed to SIWP2 allowing the free movement of the PDMS-encased serpentine, preventing strain concentration and ensuring uniform stress dispersion. In addition to unidirectional tensile testing, the electrical stability of Cu-deposited SIOP and SIWP2 was evaluated under cyclic twisting modes at 90° (Fig. 4H). SIWP2 with Cu exhibited minimal resistance changes over 1000 cycles ($R/R_0 \approx 1.41$), while SIOP with Cu showed a much higher increase in resistance ($R/R_0 \approx 5.54$). These results demonstrated the superior mechanical and electrical stability of SIWP2 in PDMS under twisting deformation, which was attributed to its ability to reduce strain concentration and achieve uniform stress distribution.

The proposed pore effect was not limited to PDMS. To verify its broader applicability, we tested Ecoflex 0020 and Ecoflex Gel, which have a lower modulus than PDMS. The SIWP2 embedded in Ecoflex 0020 and Ecoflex Gel exhibited a higher strain at failure compared to the corresponding SIOP (Fig. 5A and B). To evaluate the mechanical reliability under repeated stretching, we conducted 10 000-cycle tests (at 50% strain) and monitored the relative change in stress for both SIOP and SIWP2 embedded in Ecoflex 0020 and Ecoflex Gel. A crack was observed in SIOP embedded in Ecoflex 0020 after 8801 cycles, whereas SIWP2 maintained mechanical stability without failure throughout all 10 000 cycles (Fig. 5C). Similarly, a crack was observed in SIOP embedded in Ecoflex Gel after 3509 cycles, whereas SIWP2 maintained mechanical stability without failure throughout all 10 000 cycles (Fig. 5D). Additionally, when Ecoflex was used as the polymer matrix, we confirmed that introducing pores enhanced mechanical stability more effectively than improving the adhesion of the serpentine interconnects (Fig. S9, ESI†).

In addition to the aforementioned elastomers, both SIOP and SIWP2 were embedded in dragon skin and styrene–ethylene–butylene–styrene (SEBS). We evaluated the strain at failure at which delamination occurred at the elastomer/PI interface (Fig. S10, ESI†). The strain at failure of SIWP2 in all tested elastomers was higher than that of SIOP. Overall, the proposed SIWP2 structure significantly reinforced stretchability and durability across various materials compared to previously reported fully encapsulated serpentine interconnects (Table S1, ESI†).

The SIWP2 design is advantageous for controlling repetitive deformation in electronics and enabling various applications. One of the most promising applications of serpentine-shaped electrodes is in stretchable displays. For the demonstration, we fabricated an array of light-emitting diodes (LEDs) that could be controlled through an external power source (Fig. 6A). LEDs were placed on each rectangular polyimide island in a 2 × 3 array, with 15 mm between islands, on SIWP2 embedded in PDMS. The LEDs were encapsulated with a PDMS prepolymer solution, which cured heat to fix the chips. The LED operated at 1.75 V and each pixel exhibited consistent current–voltage characteristics and luminance under stretching (Fig. S11, ESI†). The fabricated stretchable LED array operated under three deformation modes: stretching (135%), twisting (180°), and poking. The SIWP2 structure deposited with Cu could be utilized as a stretchable heater through Joule heating (Fig. 6B). To enhance the reliability of this heater, the entire heating area of the copper on the PI substrate was encapsulated with PDMS. Real-time IR images of this SIWP2 heater from 0 V to 6 V showed a uniform temperature distribution at each voltage (Fig. 6C). This measurement was conducted by connecting a source meter to the island surfaces at both ends of SIWP2. As illustrated, the temperature of the interconnect increased monotonically with each successive 1 V increment applied to SIWP2. The average temperature of the heater was measured when the temperature reached saturation. The average temperature increased from 28 °C at 0 V to ~70 °C at 6 V and decreased back to 27 °C when the voltage was reduced to 0 V (Fig. 6D). The heater exhibited consistent periodic heating even under repetitive DC bias. The thermal stability and mechanical reliability of SIWP2 and SIOP heaters under stretching deformation are demonstrated (Fig. 6E). This heater was tested up to 30% stretching at 6 V, showing a distinctive trend in changes of average temperature. SIWP2 maintained an average temperature of 70 °C at 0–30% strains, while the temperature of SIOP decreased with increasing strain, dropping by ~20 °C at 30% compared with 0%, and displayed uneven heat distribution. This was attributed to the non-uniform heating of the PDMS

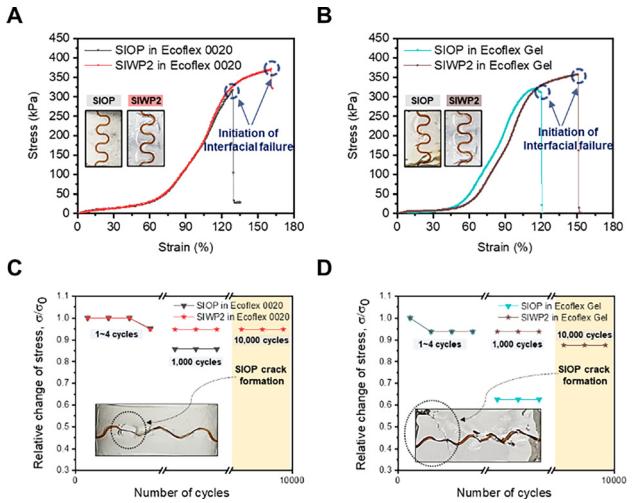

Fig. 5 Compatibility of SIWP2 with various polymer materials. (A and B) Stress–strain curves showing the stretchability of SIOP and SIWP2 in Ecoflex 0020 (A) and Ecoflex Gel (B). Insets show SIOP and SIWP2 with various polymer materials before stretching. (C and D) Relative change of stress (σ/σ_0) *versus* cycles for SIOP and SIWP2 in Ecoflex 0020 (C) and Ecoflex Gel (D) under repeated stretching of 50% strain. For SIWP2 embedded in Ecoflex 0020, crack formation was observed in SIOP after 8801 cycles whereas, in Ecoflex Gel, the SIOP structure failed due to cracking after 3509 cycles.

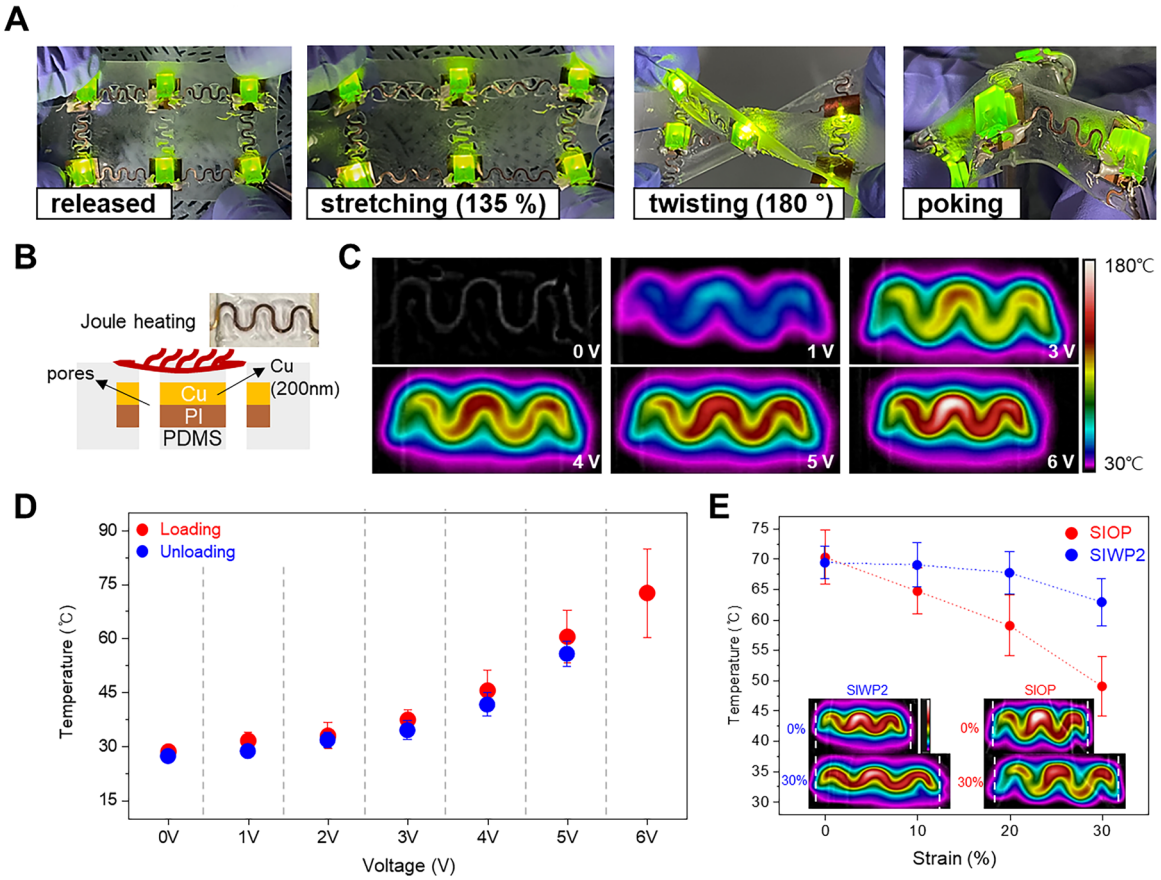

Fig. 6 Stretchable LED array withstanding various deformation modes and stretchable heater demonstrating thermal stability under mechanical deformation. (A) Photographs of a stretchable LED array capable of withstanding various deformation modes (stretching, twisting and poking). (B) Side view of the stretchable heater with SIWP2 (schematic). A 200-nm Cu layer was deposited on the PI serpentine structure, and the device was embedded in PDMS. Joule heating was achieved through electrical connections to the Cu layer. The top image shows the top view of the stretchable heater. (C) Infrared thermal imaging of SIWP2 at each voltage from 0 V to 6 V. (D) Temperature variation of the stretchable heater with SIWP2 as the voltage increased from 0 V to 6 V and then decreased back to 0 V. The red dots represent loading up to 6 V, while the blue dots represent unloading back to 0 V. (E) Comparison of the stretchable heater with SIOP and SIWP2 under strain ranging from 0% to 30%.

encapsulating the SIOP. As shown in Fig. 2, encapsulated PDMS restricted the *z*-axis movement of the serpentine under strain, making it difficult to maintain the structure and achieve uniform heating across the device.

Conclusions

A serpentine interconnect is effective for the practical implementation of stretchable devices. However, research on the long-term use of a serpentine interconnect when integrated with other polymers remains limited. In this sense, we presented geometrically designed pores to suppress interfacial cracks between a serpentine interconnect and the polymer matrix. By utilizing the strain-reduced regions created by the pores, we found that the stress on the interface decreased significantly. The optimized pores imbibed the interconnects with excellent mechanical and electrical stability under both stretching (15 000 cycles) and twisting cycles (1000 cycles). Furthermore, we demonstrated highly durable stretchable LED arrays and an electrical heater. To further optimize the fabrication process, a DIW-based 3D printing approach may be adopted to simplify manufacturing and improve productivity.

Methods

Fabrication of SIOP and SIWP with a copper coating

A PI film, 125 μm in thickness, was laser-cut (CO_2 laser cutter) to form square islands and serpentine-shaped electrode regions. The islands measured 1 cm × 1 cm, while the serpentine had a width of 5 mm and length of 30 mm (Fig. S1, ESI†). Copper was deposited onto the PI film using thermal evaporation equipment, resulting in a thickness of 200 nm. Teflon cuboids (5 cm × 3 cm × 1 cm) were laser-cut into patterns with first and second pore shapes. PDMS (Sylgard 184; Dow Corning) was spin-coated at 500 rpm for 30 s onto the Teflon mold, followed by thermal curing at 80 °C for 1 h. The PI serpentine interconnect was then placed on top, and PDMS was spin-coated at 500 rpm for 30 s, followed by an additional thermal curing at 80 °C for 1 h. Subsequently, PDMS was spin-coated at 500 rpm for 30 s, and another round of thermal curing was

performed at 80 °C for 1 h. PDMS was deposited three times. The completed SIOP or SIWP was lifted off from the Teflon molds. Ecoflex 0020 (Smooth-On), Dragon Skin 10 NV (Smooth-On) and Ecoflex Gel (Smooth-On) were also used as the elastic polymer matrix for alternative encapsulation. Part A and part B of each material were mixed in a 1 : 1 weight ratio using a planetary mixer (Thinky AR-100) for 2 min, followed by a 30-s defoaming step. Using a Teflon mold, spin-coating and curing were repeated thrice for each elastomer, in the same manner as with PDMS. The curing condition for Ecoflex Gel was 3 h at room temperature, while Ecoflex 0020 and Dragon Skin 10 NV were cured at 80 °C for 1 h. Styrene–ethylene/butylene–styrene block copolymer (SEBS; TUFTEC H1221; Asahi Kasei) was dissolved in toluene to obtain a 25 wt% solution. The solution was then cast into a Teflon mold *via* spin-coating. The latter and subsequent curing steps were repeated thrice to achieve uniform thickness, following the same process as used for PDMS-based serpentine interconnects. Each layer was cured at 80 °C for 1 h.

FE simulation of strain distribution

An FE simulation based on a linear elastic model was conducted to investigate the mechanical behaviors in SIOP, SIWP1, and SIWP2 in PDMS. The modulus and Poisson's ratio of PDMS were set to 1 MPa and 0.49, respectively, while those of PI were set to 2.5 GPa and 0.34, respectively. The strain distribution obtained from the simulation was expressed in terms of logarithmic strain under stretching.

Fabrication of a stretchable LED array and stretchable heater

To manufacture a stretchable LED array, a 2 × 3 array of SIWP was packed in a rectangular configuration. Prior to the fabrication of SIOP and SIWP, copper was coated onto the PI serpentine and encapsulated with PDMS. Subsequently, green square LEDs (Devicemart, Korea) were securely fixed onto the islands using PDMS. To power the stretchable heater and LED array, a source meter (Keithley 2400; Tektronix, USA) supplied the required voltage. Next, for the fabrication of a stretchable heater, the process of manufacturing the electrodes for SIWP was identical to that of the stretchable heater. The center-to-center distance between islands was 15 mm. Each island was connected with copper wire and encapsulated with PDMS. The source meter applied a voltage of 0 V to 6 V to the stretchable heater. Simultaneously, real-time temperature measurements were taken using an infrared thermal imaging camera (FLIR, USA).

Tensile and fatigue tests and measurement of electrical properties

Tensile and fatigue tests for SIOP and SIWP were performed using a force gauge (maximum force: 100 N, Mark-10) and a stand with a motor (Mark-10). The strain speed of the motor was set at 200 mm min^{-1} for all tests. In the fatigue test under twisting, repetitive stretching was applied to the twisted substrate. Additionally, the resistance of the stretchable electrode was measured at 1 V and 1-kHz frequency using an LCR meter (4284A; HP, USA). Electrical conductivity was measured for the Cu layer (square-pattern with 1 mm × 1 mm pad) using a four-point probe (M4P205; MSTech) and a series measuring meter (2401; Keithley). The thickness of the Cu layer was measured from SEM images using a SU5000 (Hitachi) system.

Author contributions

Seungkyu Lee: conceptualization, data curation, data analyses, investigation, methodology, visualization, and writing (original draft). Jun Chang Yang: conceptualization, data analyses, methodology, software, validation, visualization, and writing (original draft). Steve Park: funding acquisition, project administration, resources, supervision, and writing (review and editing).

Conflicts of interest

There are no conflicts of interest to declare.

Data availability

The data that support the findings of our study are available in the ESI† of this article.

Acknowledgements

This work was supported by LG Display (C2024004283_V1), the National Research Foundation of Korea (NRF) and the Korea government (MSIT) (RS-2024-00407084). This research was supported by Korea Electrotechnology Research Institute (KERI) Primary research program through the National Research Council of Science & Technology (NST) funded by the Ministry of Science and ICT (MSIT) (No. 25A01020).

References

1 N. Matsuhisa, X. Chen, Z. Bao and T. Someya, *Chem. Soc. Rev.*, 2019, **48**, 2946–2966.
2 W. C. Gao, J. Qiao, J. Hu, Y. S. Guan and Q. Li, *Responsive Mater.*, 2024, **2**, e20230022.
3 S. I. Park, Y. Xiong, R. H. Kim, P. Elvikis, M. Meitl, D. H. Kim, J. Wu, J. Yoon, C. J. Yu, Z. Liu, Y. Huang, K. C. Hwang, P. Ferreira, X. Li, K. Choquette and J. A. Rogers, *Science*, 2009, **325**, 977–981.
4 S. Park, S. Ban, N. Zavanelli, A. E. Bunn, S. Kwon, H. R. Lim, W. H. Yeo and J. H. Kim, *ACS Appl. Mater. Interfaces*, 2023, **15**, 2092–2103.
5 Y. Deng, F. Bu, Y. Wang, P. S. Chee, X. Liu and C. Guan, *npj Flexible Electron.*, 2024, **8**, 12.
6 S. Li, G. Liu, R. Li, Q. Li, Y. Zhao, M. Huang, M. Zhang, S. Yin, Y. Zhou, H. Tang, L. Wang, G. Fang and Y. Su, *ACS Nano*, 2022, **16**, 541–553.
7 T. Corrigan, P. Fleming, C. Eldredge and D. Langer-Anderson, *Commun. Mater.*, 2023, **4**, 31.

8 H. G. Park, H. C. Jeong, Y. H. Jung and D. S. Seo, *Sci. Rep.*, 2015, **5**, 12356.
9 Z. Yan, Y. Liu, J. Xiong, B. Wang, L. Dai, M. Gao, T. Pan, W. Yang and Y. Lin, *Adv. Mater.*, 2023, **35**, e2210238.
10 X. Yang, M. Zhang, M. Xie, M. Sun, H. Luo, Q. Li, X. Chen and W. Pang, *Adv. Electron. Mater.*, 2023, **9**, 2201339.
11 B. Ji, Z. Xie, W. Hong, C. Jiang, Z. Guo, L. Wang, X. Wang, B. Yang and J. Liu, *J. Materiomics*, 2020, **6**, 330–338.
12 T. Koshi, A. Takei, T. Nobeshima, S. Kanazawa, K.-I. Nomura and S. Uemura, *Flexible Printed Electron.*, 2024, **9**, 015009.
13 X. Dong, Y. Nie, H. Sun, X. Qian, M. Xu, Z. Zhang, B. Liu, Z. He, Y. Li, C. Miao and J. Liu, *ACS Appl. Electron. Mater.*, 2023, **5**, 4650–4656.
14 J. Li, X. Wu and Y. Su, *Adv. Mater.*, 2023, **35**, e2300340.
15 S. L. Jun Chang Yang, B. Soo Ma, J. Kim, M. Song, S. Yeong Kim, D. Won Kim, T.-S. Kim and S. Park, *Sci. Adv.*, 2022, **8**, eabn3863.
16 T. Pan, M. Pharr, Y. Ma, R. Ning, Z. Yan, R. Xu, X. Feng, Y. Huang and J. A. Rogers, *Adv. Funct. Mater.*, 2017, **27**, 1702589.
17 Y. Su, X. Ping, K. J. Yu, J. W. Lee, J. A. Fan, B. Wang, M. Li, R. Li, D. V. Harburg, Y. Huang, C. Yu, S. Mao, J. Shim, Q. Yang, P. Y. Lee, A. Armonas, K. J. Choi, Y. Yang, U. Paik, T. Chang, T. J. Dawidczyk, Y. Huang, S. Wang and J. A. Rogers, *Adv. Mater.*, 2017, **29**, 1604989.
18 M. Han, H. Wang, Y. Yang, C. Liang, W. Bai, Z. Yan, H. Li, Y. Xue, X. Wang, B. Akar, H. Zhao, H. Luan, J. Lim, I. Kandela, G. A. Ameer, Y. Zhang, Y. Huang and J. A. Rogers, *Nat. Electron.*, 2019, **2**, 26–35.
19 J. A. Fan, W. H. Yeo, Y. Su, Y. Hattori, W. Lee, S. Y. Jung, Y. Zhang, Z. Liu, H. Cheng, L. Falgout, M. Bajema, T. Coleman, D. Gregoire, R. J. Larsen, Y. Huang and J. A. Rogers, *Nat. Commun.*, 2014, **5**, 3266.
20 S. Xu, Y. Zhang, J. Cho, J. Lee, X. Huang, L. Jia, J. A. Fan, Y. Su, J. Su, H. Zhang, H. Cheng, B. Lu, C. Yu, C. Chuang, T. I. Kim, T. Song, K. Shigeta, S. Kang, C. Dagdeviren, I. Petrov, P. V. Braun, Y. Huang, U. Paik and J. A. Rogers, *Nat. Commun.*, 2013, **4**, 1543.
21 R. Jiao, R. Wang, Y. Wang, Y. K. Cheung, X. Chen, X. Wang, Y. Deng and H. Yu, *Microsyst. Nanoeng.*, 2023, **9**, 149.
22 K. I. Jang, K. Li, H. U. Chung, S. Xu, H. N. Jung, Y. Yang, J. W. Kwak, H. H. Jung, J. Song, C. Yang, A. Wang, Z. Liu, J. Y. Lee, B. H. Kim, J. H. Kim, J. Lee, Y. Yu, B. J. Kim, H. Jang, K. J. Yu, J. Kim, J. W. Lee, J. W. Jeong, Y. M. Song, Y. Huang, Y. Zhang and J. A. Rogers, *Nat. Commun.*, 2017, **8**, 15894.
23 Y. Shi, J. Zhao, B. Zhang, J. Qin, X. Hu, Y. Cheng, J. Yu, J. Jie and X. Zhang, *Adv. Mater.*, 2024, **36**, e2313603.